



HAL
open science

Submarine hull integrity under blast loading

Bertrand Langrand, Nicolas Leconte, Aude Menegazzi, Thierry Millot

► **To cite this version:**

Bertrand Langrand, Nicolas Leconte, Aude Menegazzi, Thierry Millot. Submarine hull integrity under blast loading. *International Journal of Impact Engineering*, 2009, 36 (8), pp.1070. 10.1016/j.ijimpeng.2009.03.001 . hal-00587978

HAL Id: hal-00587978

<https://hal.science/hal-00587978>

Submitted on 22 Apr 2011

HAL is a multi-disciplinary open access archive for the deposit and dissemination of scientific research documents, whether they are published or not. The documents may come from teaching and research institutions in France or abroad, or from public or private research centers.

L'archive ouverte pluridisciplinaire **HAL**, est destinée au dépôt et à la diffusion de documents scientifiques de niveau recherche, publiés ou non, émanant des établissements d'enseignement et de recherche français ou étrangers, des laboratoires publics ou privés.

Accepted Manuscript

Title: Submarine hull integrity under blast loading

Authors: Bertrand Langrand, Nicolas Leconte, Aude Menegazzi, Thierry Millot

PII: S0734-743X(09)00056-6

DOI: [10.1016/j.ijimpeng.2009.03.001](https://doi.org/10.1016/j.ijimpeng.2009.03.001)

Reference: IE 1761

To appear in: *International Journal of Impact Engineering*

Please cite this article as: Langrand B, Leconte N, Menegazzi A, Millot T. Submarine hull integrity under blast loading, *International Journal of Impact Engineering* (2009), doi: 10.1016/j.ijimpeng.2009.03.001

This is a PDF file of an unedited manuscript that has been accepted for publication. As a service to our customers we are providing this early version of the manuscript. The manuscript will undergo copyediting, typesetting, and review of the resulting proof before it is published in its final form. Please note that during the production process errors may be discovered which could affect the content, and all legal disclaimers that apply to the journal pertain.



Submarine hull integrity under blast loading

Bertrand Langrand^(a), Nicolas Leconte^(a), Aude Menegazzi^(b) and Thierry Millot^(c)

(a) French Aerospace Lab (ONERA)
Aeroelasticity and Structural Dynamic Department
5, boulevard Paul Painlevé, 59045 Lille Cedex, France
tel. +33(0)3.20.49.69.79 – fax. +33(0)3.20.49.69.55
e-mail: bertrand.langrand@onera.fr (*corresponding author*)

(b) French Ministry of Defence (DGA)
DET/CEP/MC/PMA
5-7, rue des Mathurins, 92221 Bagneux Cedex, France

(c) French Military Shipyard (DCNS)
CESMAN/RDMPC
Indret BP30, 44620 La Montagne, France.

Key-words—Explosion; ECST; Welded Panel; FEM

Abstract—The paper deals with numerical methodologies to model and study the structural resistance of submarine hull against explosions, where fluid and solid phenomena interact. Explosion Crack Starter Tests (ECST), which are a standard procedure to study submarine materials and weldments with respect to blast loading, are modelled using an explicit FE code that solves Fluid/Structure (F/S) interactions within the same computation. The proposed numerical methods aim at computing the structural response of a target subjected to sequential explosions. Numerical results are compared to the corresponding explosion tests (ECST) performed by DGA (French Ministry of Defence).

1 Introduction

The literature survey highlights that there exists several experimental procedures to study submarine materials and weldments with respect blast loading. Among them Bulge Explosion Tests (BET), Explosion Crack Starter Tests (ECST) and Underwater Bulge Explosion testing (UBE) can be distinguished. BET and ECST are standard

experiments normally used to assess the plastic strain capability of structural metallic materials and welded assemblies with respect to submarine explosion problems although that kind of tests considers air environment instead of water [1,2]. In these tests, several shots (two at the minimum) are undertaken sequentially to study the strength of submarine hulls under blast loading conditions. Tests may be also performed at different temperatures to define the Fracture Transition for Plastic loading (FTP). Explosion tests acceptance criteria are synthesised in Table 1. Underwater Bulge Explosion testing (UBE) has also been developed for assessment of a welding consumable [3]. Underwater explosions produce the combined effects of shock and bubble (expand and collapse) on naval structures that are quite different from air blast.

From a numerical standpoint, the literature shows that most of the blast-loaded structure computations (that features large transformations) are performed using structural FE codes. The computations we focus on take into account the non-linear behaviour of the problem (geometrically and materially). The explosion loading is either applied to the structure through empirical laws [4–10] or pressure gauge measurements [11–13]. The pressure loading from the explosive charge is assumed to be a rectangular pulse uniformly distributed over the plate surface [4–8] or is idealised as triangular [13–14] or exponentially decaying empirical laws [9–10,12]. A new tendency seems to appear with the fully coupled fluid/structure models where the detonation of the explosive, the air blast shock propagation, the interaction of the blast with the structure and the structure response are computed [15–16], which must be caused by the need of a closer representation of physical phenomena and the rise of computational power.

The paper deals with fully coupled Fluid/Structure simulations of ECST tests, taking into account the ductile behaviour of experimented plates (Continuous Damage Mechanics and not Fracture Mechanics). The paper aims at developing numerical methods to model the behaviour of metallic welded structures subjected to sequential explosion pressure waves. First, metallic samples are tested to study the strain rate sensitivity of the Fusion Zone (FZ), Heat Affected Zone (HAZ) and Base Metal (BM) materials, and to identify the parameters of viscoplastic models (homogeneous) used in FE computations. Then, based on ECST procedure, a first explosion simulation is computed until complete dynamic relaxation. Numerical methodologies are developed to (1) capture the deformed shape of the metallic plate and (2) measure the residual plastic strain and stress fields in all 3D FE of the metallic plate. The deformed shape (including fluid domain local re-meshing for F/S interaction) and the residual properties (plastic strain and stress tensor components) of the metallic plate are finally introduced as an initial state of a second explosion simulation. Numerical results are compared to the corresponding explosion tests (ECST) performed by DGA.

2 Characterisation of welded “materials” viscoplastic behaviour

Based on a micro hardness diagram, to locate the fusion zone and the average heat affected zone, metallic tensile test specimens (Figure 1) are extracted from a welded flat panel. FZ and HAZ material specimens are machined in a welded plate: FZ specimens in the weldment area and HAZ outside, at 24mm distance (Figure 1). The specimen geometry is adapted to static, hydraulic jack and Hopkinson bar tests [17]. The sample material is considered homogeneous (for BM, FZ and HAZ) due to the small size of specimens.

Experiments are undertaken at ambient temperature and -5°C (flat panel temperature for the explosion tests considered in the paper). Pre-test FE simulations were performed to assess the flat panel strain rate range during the explosion test. Maximum strain rate levels were found to be up to 400s^{-1} . Tensile tests are performed on a hydraulic jack, using a specific experimental device [17], at several velocities for each specimen temperature. The force is measured with a piezoelectric cell (Kistler) and the global strain with an optical extensometer (Zimmer).

The experimental analysis shows that mechanical behaviours are very close for both HAZ and BM materials whatever the strain rate or temperature (Figure 2).

Consequently, the explosion FE model could be simplified by neglecting the influence of the HAZ material. The influence of temperature (-5°C) may also be neglected during the identification procedure of material constitutive models if necessary. Figure 3 presents raw (unfiltered) engineering stress/strain diagrams.

3 Explosion Crack Starter Tests FE simulations

Explosion Crack Starter Tests were developed from 1949 to 1950 and have been used extensively to investigate the factors, which determine the performance of weldments, particularly in submarine structure, and other large welded structures [1,2]. This standard explosion test is principally used to qualify prospective products wherein a flat test plate specimen is explosively loaded into a circular test die. A deposited and notched defect (or crack starter bead) is machined on the flat panel (Figure 4). The crack starter is a brittle weld metal deposited on the weldment to present a sharp crack front to the weld or HAZ or base metal for the purpose of assessing the resistance to cracking of the material being tested.

The flat panel thickness governs the explosion test parameters. For a 50mm thick flat panel, the dimensions are: flat panel length: 600mm square, test die internal diameter: 400mm, stand-off-distance: 350mm, charge diameter/weight: 400mm/10kg. The crack starter geometrical characteristics are as follow: length $L = 75\text{mm}$, width $w = 12\text{mm}$, overall thickness $e = 8\text{mm}$, distance crack tip/test plate $h = 5\text{mm}$ (Figure 4a).

Experimental observation of the welded panels (tested at -5°C) has not highlighted a substantial crack propagation emanating from the crack starter after explosion tests. The crack propagation has only a weak influence on the test plate deflection, which is mainly triggered by material plastic strain process. To simulate the stress concentration (that will trigger damage and failure process) at the V-shape notch tip (Figure 4a), it would be necessary to mesh the crack starter and a portion of the plate (in the case of a regular mesh) with a very detailed mesh, which would lead to a too CPU consuming model. For both these reasons, it has been decided not to consider the influence of the crack starter in the following simulations. However, for very low temperature conditions (e.g. -70°C) the crack propagation might be a more crucial problem and the influence of the crack starter will no more be negligible.

The metallic panel features an “initial” flatness defect due to the welding process (8mm deflection measured at the panel centre). A 3D digitiser, which is an optical measuring system based on the principle of triangulation, is used to digitalise the specimen. Projected fringe patterns are observed with two cameras. 3D coordinates for each camera pixel are calculated and the complete 3D data sets are exported [18]. The specimen digitalisation is performed to mesh the panel and to investigate on the effects of the flatness defect on its behaviour (in comparison with an ideally flat panel).

Due to the flatness defect, no symmetry boundary condition can be considered for FE simplification, and complete 3D FE models have to be computed. The size of the finite elements is fixed to 10mm and 5mm in the fluid and solid domains, respectively. With such element sizes, the number of FE is already about 435 000 (360 000 FE for the fluid area and 75 000 FE for the solid area) and the elementary time step is $2.5 \cdot 10^{-5}$ ms. Due to the element sizes, the material failure is not considered in the following simulations.

The modelling method used in Radioss FE code for the fluid medium is based on an Arbitrary Lagrange Euler formulation (ALE). The fluid domain is split into several areas: the explosive, the air and a silent boundary (Figure 4b). The behaviour of the fluid material in the explosive and the air areas is modelled using a viscous hydrodynamic law (1). The silent boundary prevents wave reflections at the edge of the fluid mesh. Its behaviour is similar to a low-pass filter (2) where l_c ($l_c=500$ mm) is a characteristic length that defines a cut frequency (about 50Hz in these computations).

$$p = C_0 + C_1\mu + C_2\mu^2 + C_3\mu^3 + (C_4 + C_5\mu)E_0 \quad (1)$$

with $\mu = \rho/\rho_0 - 1$.

$$\frac{\partial p}{\partial t} = \rho c \left(\frac{\partial V_n}{\partial t} - V_n \cdot \text{div}(\vec{V} - V_n \cdot \vec{n}) \right) + c \frac{p_\infty - p}{2l_c} \quad (2)$$

with $f_c = \frac{c}{4\pi l_c}$ and $c = \sqrt{E/\rho}$.

In the case of a perfect gas, the relation (1) may be simplified in (3) and the parameters are then defined as a function of the perfect gas constant, γ . The initial condition of the explosion is based on an energy deposit (and its propagation) in the FE located in the mesh area of the explosive. The elementary initial energy, E_0 , of the viscous

hydrodynamic law is set to the detonation energy, E , of the Jones-Wilkins-Lee (JWL) equation of state (EOS) (4) [19], which has been completely characterised for numerous explosives [20]. The density of the explosive can also be found in the B.M. Dobratz handbook [20]. This modelling method has been validated for several explosives by pressure profiles comparison with a detonation oriented fluid code [21]. All material constants used for the modelling of the explosive and the air are collected in Table 2.

$$p = (C_4 + C_5\mu)E_0 \quad (3)$$

$$\text{with } \begin{cases} C_4 = C_5 = \gamma - 1 \\ E_0 = p_0 / (\gamma - 1) \end{cases} \text{ for the air area,}$$

$$\text{and } \begin{cases} C_4 = C_5 = \gamma - 1 \\ E_0 = E \end{cases} \text{ for the explosive area.}$$

$$p = A \left(1 - \frac{\omega}{R_1} V \right) e^{-R_1 V} + B \left(1 - \frac{\omega}{R_2} V \right) e^{-R_2 V} + \frac{\omega}{V} E \quad (4)$$

The test plate is split into two material areas (Figure 4b): one for the FZ material and another for the BM material (HAZ material influence is neglected according to experimental results of section 2). The dimensions and the shape of the FZ area have been determined according to the manufacturing preparation of the plate before welding process (Figure 1c). The material behaviour is modelled with a Johnson-Cook model (5) [22]. The viscoplastic parameters are identified for both base metal and fusion zone materials, using experimental results obtained in section 2. Parameter A is set to the yield stress and parameters (B, n) are defined by equation: $\ln(\sigma - A) = \ln(B) + n \ln(\epsilon_p)$ that best correlates quasi-static experimental results until necking ($d\sigma/d\epsilon = 0$) [23].

Parameter C is set to the slope of $\left[\frac{\sigma(\dot{\epsilon})}{\sigma(\dot{\epsilon}_0)} - 1 \right] = C \ln \left(\frac{\dot{\epsilon}}{\dot{\epsilon}_0} \right)$ that best correlates dynamic

experimental results. The identified parameters are collected in Table 3. Johnson-Cook model parameters have also been validated using FE models of the experimented tensile samples and welded coupons (static and dynamic imposed displacements are considered in the validation step, as well as several mesh size are investigated). The test die is made of steel and its behaviour is assumed linear and elastic in the following computations.

$$\sigma = \left(A + B \varepsilon_p^n \right) \cdot \left(1 + C \ln \frac{\dot{\varepsilon}}{\dot{\varepsilon}_0} \right) \quad (5)$$

3.1 First ECST FE simulation

The first ECST FE simulation consists in a set of two computations. During computation n°1 ($0 < T < 1\text{ms}$), the complete fluid/structure interaction problem is solved until the flat panel starts its spring-back (detected by numerical strain gauges). The test plate centre peak overpressure is about 10 000bars and its maximum acceleration is about 250 000g (Butterworth -4db filter).

Computation n°2 ($1\text{ms} < T < 2\text{ms}$) consists in a dynamic relaxation calculation to define residual properties of the flat panel: plastic strain and stress tensor in each FE, maximum deflexion and thickness reduction. The whole fluid mesh is deleted in this second computation to save computational cost. The residual properties will initialise the second ECST FE simulation: (1) geometry of the deformed flat panel and (2) stress tensor and plastic strain of all 3D FE of the test plate.

At the end of the computations, thickness reduction is about 3.7% and residual plastic strain is about 17% at the centre of the test plate. Compared to material percentage elongation (15% and 14% for BM and ZF respectively), failure could appear and

propagate, all the more as the crack starter effects are not taken into account in the current FE simulation. Maximum deflection is about 40mm.

DGA performed the corresponding explosion test. Residual strain measurement is carried out using electro-erosion marked grid located on the test plate. Residual strain distribution is measured using image digitalisation and stereo correlation (for 3D measurements) systems [24]. Thickness reduction is about 4.2% and maximum deflection is about 45mm.

Figure 5 shows the residual plastic strain distribution coming from the FE simulation and the residual major strain distribution measured after the explosion experiment. To make a fair comparison between experiment and FE simulation, experimental results need to be analysed in terms of residual plastic strain using relation (6). To this aim the residual plastic strain tensor components ϵ_{ij}^p are defined by the measured major, minor strains and the thickness reduction [23]. Results are then compared in two sections of the flat panel (Figures 6). Maximum deviation between experimental and FE results is located in the welded area (Figure 6). It can be seen that FE results are satisfactory enough –in terms of local strain distribution or global deflection and thickness reduction– to process the second explosion simulation.

$$\epsilon_p = \sqrt{\frac{2}{3} \text{Tr}(\epsilon_{ij}^{p2})} \quad (6)$$

with ϵ_{ij}^p the plastic strain tensor.

The influence of the initial flatness defect (that need a 3D digitalisation to be modelled) is investigated too. Another FE simulation of the first explosion test is performed

considering an ideally flat panel FE model (without considering the initial flatness defect) instead of the previous digitalised plate FE model (considering the initial flatness defect coming from the welding process). Comparing the FE results of both simulations show that no matter if the initial flatness defect is taken into account or not, the pressure and acceleration fields are close. However, strains decrease a little in the case of the ideally flat panel.

3.2 Second ECST simulation

In-house developed programs are implemented to capture the residual deformed shape of the test plate from the last state ($T = 2\text{ms}$) of the first ECST simulation. The deformed test plate is then interfaced with the test die and the fluid mesh is locally modified for Fluid/Structure interaction (modelled using a specific tied interface). Other programs developed to handle ASCII output files from Radioss are implemented to initialise all test plate FE with plastic strain and stress tensor from the last state ($T = 2\text{ms}$) of the first ECST simulation. When this modelling process is completed, the second ECST simulation is launched in two steps as presented in section 3.1 and illustrated in Figure 7. Material EOS and parameters are identical to the first explosion simulation (section 3).

Pressure fields measured for both explosions (ECST n°1 and 2) are very close in terms of peak overpressure, pressure rate or duration (Figure 8). Only the arrival time of the blasting wave has increased in the second ECST simulation due to the initial deformation of the test plate (initial deflection: 40mm). As pressure fields from first and second explosions are quite the same, Fluid/Structure coupling effects are very low in this case because the shape of the panel does not modify the pressure profile. It is then

possible to measure the pressure field distribution with a preliminary computation (a fluid code if considering rigid test plate), and to apply this pressure field as equivalent loading conditions for structural computations [21]. In such conditions, Fluid FE can thus be deleted for structural computations to save computational cost.

Strain distribution is localised at the test plate centre and near the test plate/test die interface (Figure 9). The strain gradient between initial and final state of the simulation is more important in the hold-on region (8% at the beginning of second explosion simulation and 18% at the end of second explosion simulation: $\Delta = 10\%$). Strains have not increased so much in the bulge region (17% at the beginning of second explosion simulation and 22% at the end of second explosion simulation: $\Delta = 5\%$). On the top face of the test panel, plastic strain are more localised following the diagonal direction of the plate (Figure 9 top left). On the top face, strain distribution is influenced by the specimen geometry (corner effects). On the top face, strains are not really isotropic as observed on the bottom face even in the hold-on region (Figure 9 bottom left).

FE model seems to overestimate the strain levels in the weld area. However experimental and numerical strain distributions are close (Figure 10). The thickness reduction due to the second explosion is about 4.7%. For overall explosion simulations, thickness reduction is about 8% (9% measured after two experimental shots). The maximum deflection measured at the end of the computation is 66mm (67mm measured experimentally).

However, acceleration measured at the test plate centre reaches 300 000g at the maximum. Shock spectrum analysis [25] shows that the second explosion test is more

severe in the high frequency range ($f > 100\text{kHz}$, Figure 11). That difference is investigated in the following parametric sensitivity study.

3.3 Discussion

The parametric study aims at analysing the influence of residual plastic strain or stress tensor (coming from the first explosion computation) introduced in all test plate FE of the second ECST simulation. Starting from the results of a first explosion simulation in terms of test plate deformed geometry, a second explosion simulation is undertaken with and without taking into account the residual stress and/or plastic strain fields of first explosion simulation for the test plate FE.

When the second ECST simulation does not consider any residual plastic strain field, the residual deflection of the test plate increases by 6% (70mm instead of 66mm). On the contrary, whether residual stresses are taken into account or not, the residual deflection of the test plate remains approximately the same.

At the end of the first explosion simulation, the test plate is in static equilibrium. However, the introduction of the residual stress field in the second explosion simulation leads to initial numerical instabilities (that looks like high frequency vibrations on the acceleration signal, Figure 12). The magnitude of these oscillations is low compared to the acceleration generated by the blasting wave but is significant enough to increase artificially the severity of the shock spectrum in the high frequency range (Figure 11).

Finally, the parametric study shows that residual plastic strains have an important influence on the residual deflection of the test plate. The severity of the second explosion test observed in section 3.2 in the high frequency range is probably due to

numerical instabilities coming from the introduction of residual stress fields in the second explosion simulation.

4 Conclusion

The paper deals with numerical methodologies (based on explicit FE codes) to model and study the structural resistance of submarine hull against sequentially explosions. Numerical results, obtained for Explosion Crack Starter Tests, are close to experiments in terms of global residual deflection, thickness reduction and local residual strain distribution. A parametric study shows that the residual plastic strains (introduced in all the FE of the test plate) have an influence on the residual deflection of the target. On the contrary the residual stresses have a weak influence on the behaviour of the test plate. Analysis has shown numerical instabilities that could explain the severity of the second explosion computation in the high frequency range. The method developed to take into account residual stresses must be improved insofar, when dealing with crack opening and propagation, residual stresses may have a more significant influence compared to a “pure” plastic deformation process. Moreover, FE results show an influence of the weldment on the strain distribution, and therefore the interest in taking into account the material behaviour of the Fusion Zone in the FE computations. This influence can be investigated in further Research by going on with the parametric FE study.

The numerical methods, developed to model the effects of a second explosion, can be reiterated to study the effects of sequential explosions on a ship hull. Moreover, it has been shown that the FE model could be simplified by applying equivalent loading conditions to save computational cost (numerous FE of the fluid domain can be deleted for structural computations in such conditions).

A perspective is to apply developed FE methods to other cases exhibiting high failure propagation (e.g. for very low temperature conditions). It would be then necessary to consider the influence of the crack starter and to model material failure. Based on material dynamic tensile tests, failure criterion from Continuous Damage Mechanics Theory (e.g. a critical plastic strain or damage) could be characterised for a specific mesh size using inverse method. Another solution could consist in applying Extended Finite Element Method [26–27], and therefore failure criterion from Fracture Mechanics Theory (e.g. static and/or dynamic stress intensity factors), once plasticity is implemented (and validated) in X-FEM codes [28].

Another aspect of the real problem consists in dealing with underwater explosion test simulations. Specific bi-phasic liquid/gas (or more generally multi-material) constitutive model has been implemented in explicit FE codes [29] that could be applied to underwater explosion problems, to assess the capability of such fluid FE model to propagate the shock pressure wave within the water and to simulate the bubble pulse. Once underwater explosion simulation validated, it could be possible to state about the relevance of ECST and BET tests to study submarine hulls.

Acknowledgements—This work has been funded by the French Ministry of Defence (DGA/SPN) and the French military shipyard (DCNS).

References

- [1] W.S. Pellini. Principals of structural integrity technology. Naval Research Laboratory, Washington DC 20375, 1976.

- [2] Department of Defense. Test Method Standard, Standard procedures for explosion testing ferrous and non-ferrous metallic materials and weldments. MIL-STD-2149A(SH), 2 February 1990.
- [3] D. Elliott. Development of an underwater bulge explosion test – Further progress. Ministry of Defence, Admiralty Research Establishment, DN (USS) 88203, June 1988.
- [4] M.D. Olson, G.N. Nurick, and J.R Fagnan. Deformation and rupture of blast-loaded square plates – Predictions and experiments, *Int. J. of Impact Engineering* 1993;13:279–291.
- [5] G.N. Nurick, M.D. Olson, J.R Fagnan and A. Levin. Deformation and tearing of blast-loaded square plates, *Int. J. of Impact Engineering* 1995;16:273–291.
- [6] G.N. Nurick, M.E. Gelman and N. S. Marshall. Tearing of blast loaded plates with clamped boundary conditions, *Int. J. of Impact Engineering* 1996;18:803–827.
- [7] N.S. Rudrapatna, R. Vaziri, and M. D. Olson. Deformation and failure of blast loaded square plates, *Int. J. of Impact Engineering* 1999;22:449–467.
- [8] N.S. Rudrapatna, R. Vaziri, and M. D. Olson. Deformation and failure of blast loaded stiffened plates, *Int. J. of Impact Engineering* 2000;24:457–474.
- [9] K. Ramajeyathilagam, C.P. Vendhan, and V. Bhujanga Rao. Non-linear transient dynamic response of rectangular plates under shock loading, *Int. J. of Impact Engineering* 2000;24:999–1015.
- [10] C. Wu, and H. Hao, Numerical simulation of structural response and damage to simultaneous ground shock and airblast loads, *Int. J. of Impact Engineering* 2007;34:556–572.

- [11] L.A. Louca, Y.G. Pan, and J.E. Harding. Response of stiffened and unstiffened plates subjected to blast loading, *Engineering Structures* 1998;20:1079–1086.
- [12] A.C. Jacinto, R.D. Ambrosini, and R.F. Danesi. Experimental and computational analysis of plates under air blast loading, *Int. J. of Impact Engineering* 2001;25:927–947.
- [13] J.W. Boh, L.A. Louca, and Y.S. Choo. Numerical assessment of explosion resistant profiled barriers, *Marine Structures* 2004;17:139–160.
- [14] J.W. Boh, L.A. Louca, and Y.S. Choo, Strain rate effects on the response of stainless steel corrugated firewalls subjected to hydrocarbon explosions, *Journal of Constructional Steel Research* 2004;60:1–29.
- [15] R. Kalavalapally, R. Penmetsa, and R. Grandhi. Multidisciplinary optimization of a lightweight torpedo structure subjected to an underwater explosion, *Finite Elements in Analysis and Design* 2006;43:103–111.
- [16] J.T. Baylot, and T.L. Bevins. Effect of responding and failing structural components on the airblast pressure and loads on and inside the structure, *Computers and Structures* 2007;85:891–910.
- [17] G. Haugou, E. Markiewicz, and J. Fabis. On the use of the non direct tensile loading on a classical split Hopkinson bar apparatus dedicated to sheet metal specimen characterisation. *Int. J. of Impact Engineering* 2006;32:778–798.
- [18] GOM ATOS theory and user manual, 2006.
- [19] E.L. Lee, M. Finger, and W. Collins. JWL equation of state coefficients for high explosives. Lawrence Livermore Laboratory, University of California, Report n° UCID-16189, 1973.

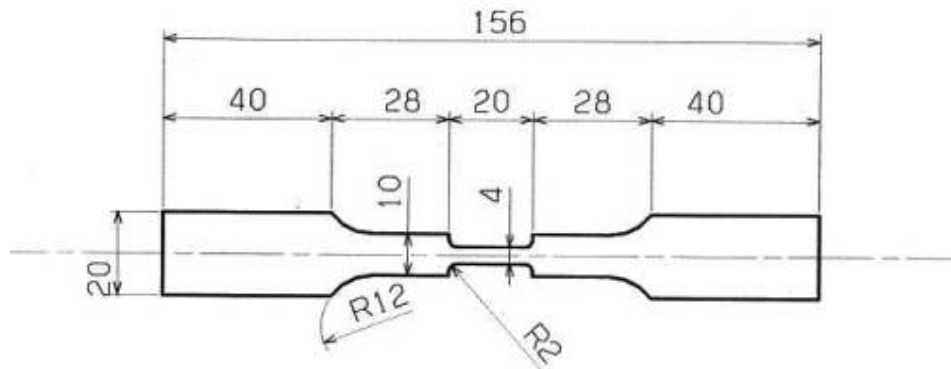
- [20] B.M. Dobratz. LLNL explosive handbook – Properties of chemical explosives and explosives simulants. Lawrence Livermore Laboratory, University of California, Report n° UCRL-52997, 1981.
- [21] B. Langrand, E. Deletombe, et al. Armoured vehicles subject to mine explosions – An analysis method for operationability and survivability. *J. Phys. IV* 2003;110:621–626.
- [22] G.R. Johnson, and W.H. Cook. A constitutive model and data for metal subjected to large strains, high strain rates and high temperatures. In Proc. of 7th *Symp. on ballistics*, The Hague, The Netherlands, 1983, p. 541–547.
- [23] J. Lemaitre, and J.L. Chaboche. *Mechanics of Solid Materials*, 2nd Edition, Dunod, 2004.
- [24] GOM ARAMIS theory and user manual, 2006.
- [25] C. Lalanne. *Chocs mécaniques – Tome 2*. HERMES Science Publication, 1st Edn., 1999.
- [26] N. Moës, J. Dolbow, and T. Belytschko. A finite element method for crack growth without remeshing. *Int. J. for Numerical Methods in Engineering* 1999;46:131–150.
- [27] J. Réthoré, A. Gravouil, and A. Combescure. A combined space-time extended finite element method. *Int. J. for Numerical Methods in Engineering* 2005;64:260–284.
- [28] T. Elguedj, A. Gravouil, and A. Combescure. Appropriate extended functions for X-FEM simulation of plastic fracture mechanics. *Computer Methods in Applied Mechanics Engineering* 2006;195(7-8):501–515.

- [29] B. Langrand, A-S. Bayart, Y. Chauveau, E. Deletombe. Assessment of multi-physics FE methods for bird impact modelling – Application to a metallic riveted airframe. *Int. J. of Crashworthiness* 2002;7(4):415–428.

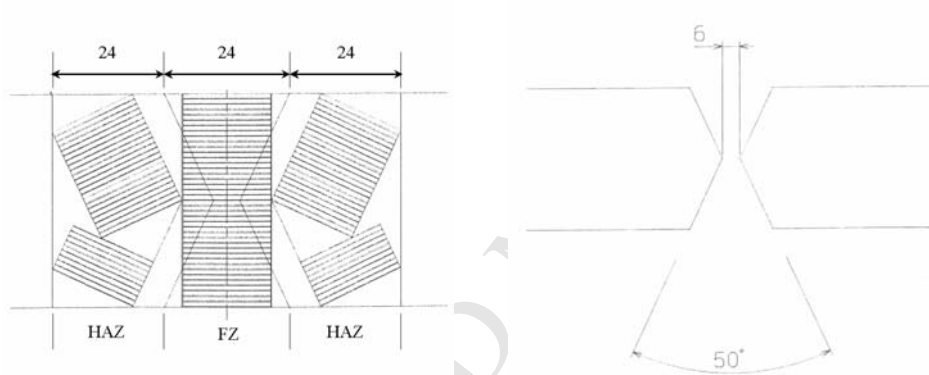
ACCEPTED MANUSCRIPT

List of Figures

- Figure 1. Tensile test specimen (all dimensions in mm – 1mm thick).
- Figure 2. Stain rate and temperature effects on welded materials mechanical properties.
- Figure 3. Measured engineering stress/strain diagram (unfiltered).
- Figure 4. Explosion Crack Starter Test.
- Figure 5. Residual strain distribution after first explosion (FEA: plastic strain – experiment: major strain).
- Figure 6. Residual plastic strain comparison (ECST n°1).
- Figure 7. Methodology for second ECST simulation.
- Figure 8. Pressure field measured at the target centre.
- Figure 9. Residual strain distribution after the second explosion (FEA: plastic strain – experiment: major strain).
- Figure 10. Residual plastic strain comparison (ECST n°2).
- Figure 11. Influence of residual properties on shock spectrum.
- Figure 12. Influence of residual properties on acceleration time history.

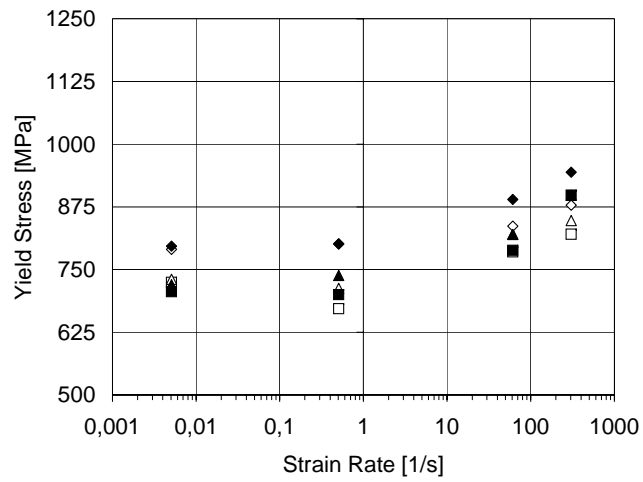


(a) specimen geometry (all dimensions in mm – 1mm thick)

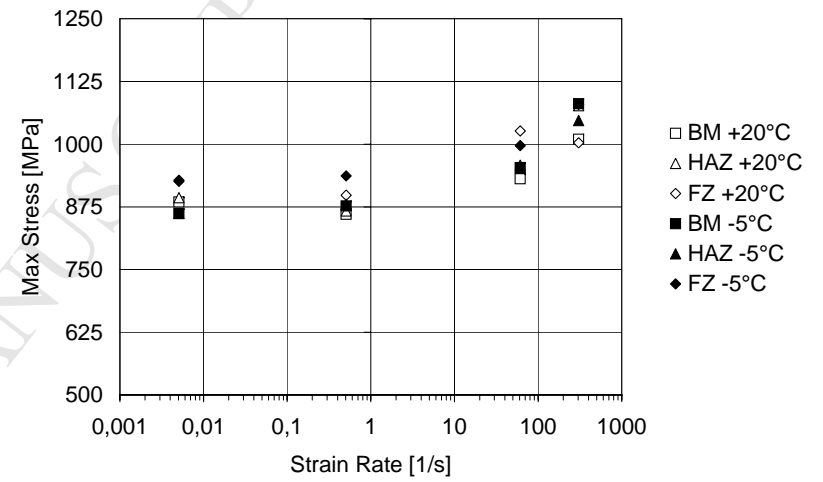


(b) cutting plan (c) manufacturing preparation before welding (double V)

Figure 1. Tensile test specimens.



(a) yield stress



(b) maximum stress

Figure 2. Stain rate and temperature effects on welded materials mechanical properties.

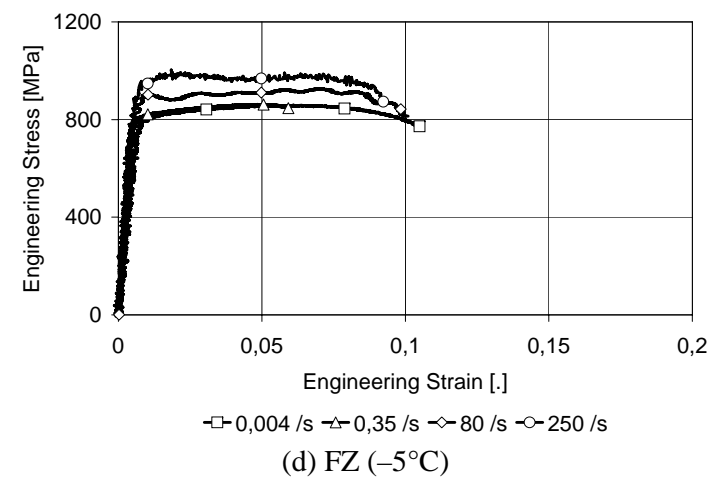
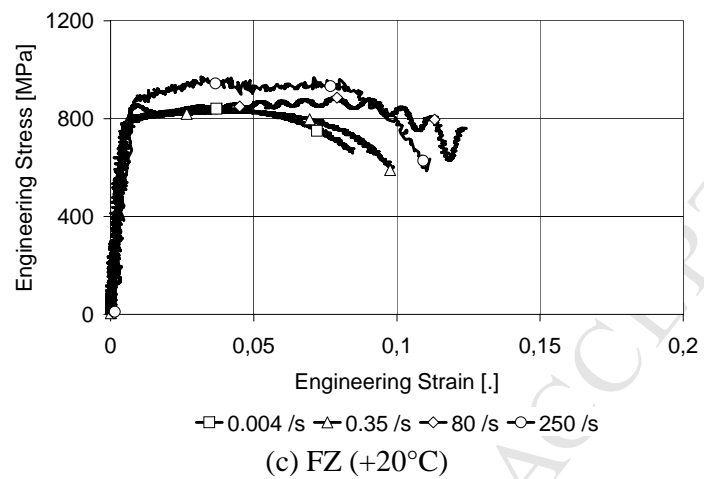
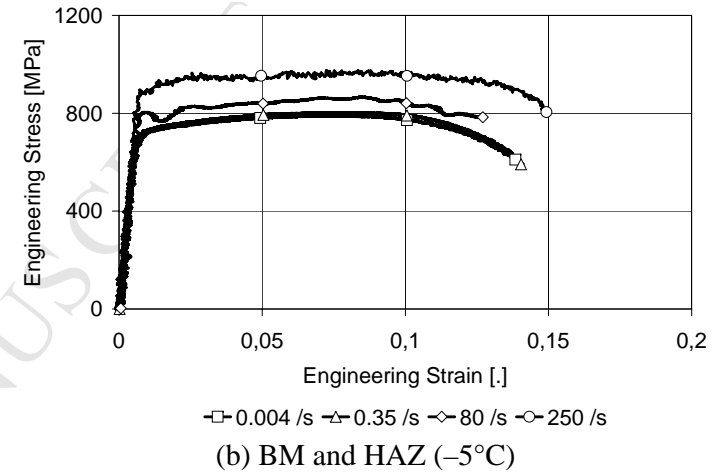
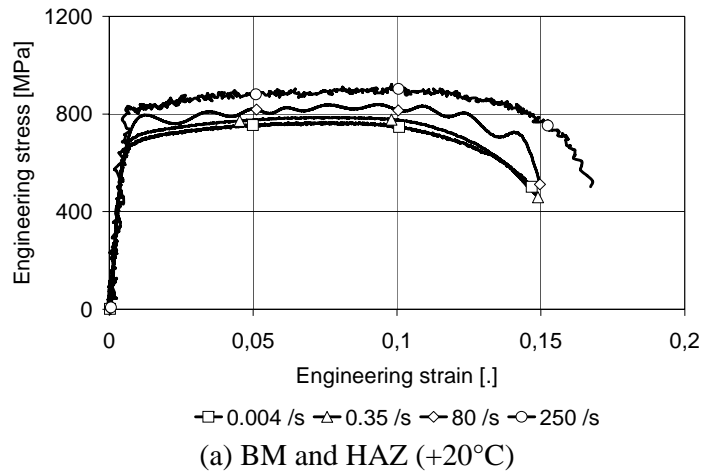
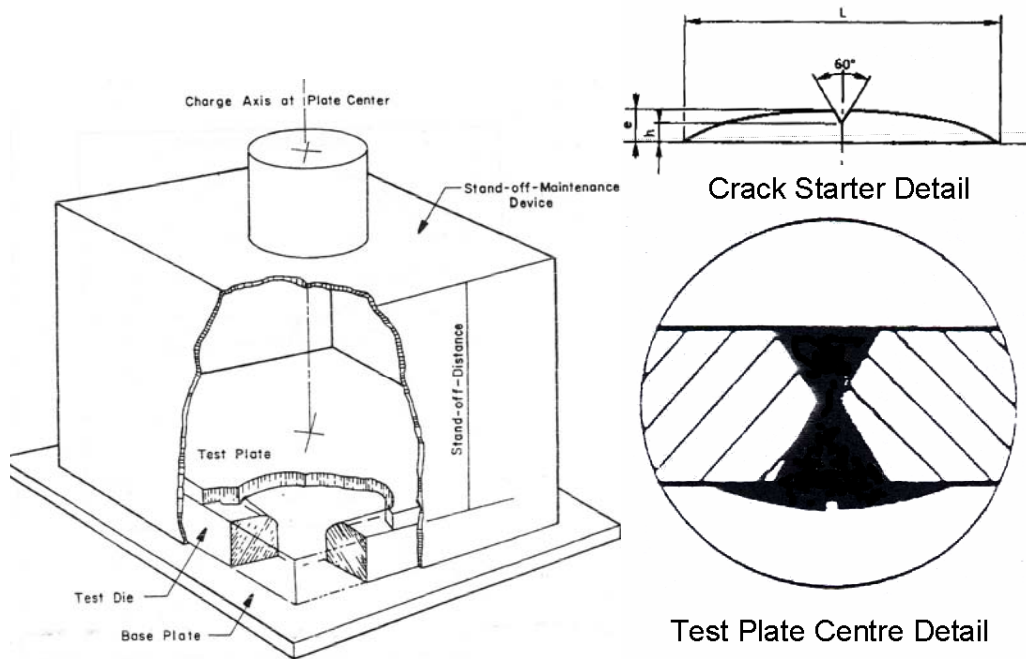
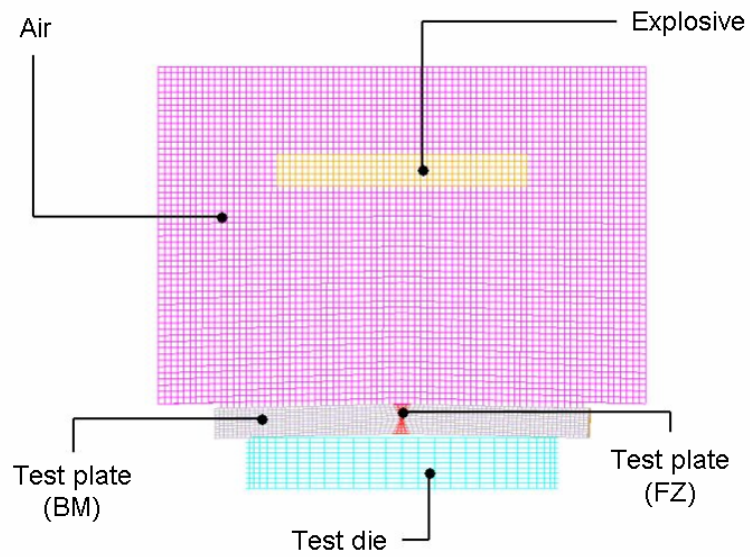


Figure 3. Measured engineering stress/strain diagram (unfiltered).



(a) Experimental configuration



(b) FE Model

Figure 4. Explosion Crack Starter Test.

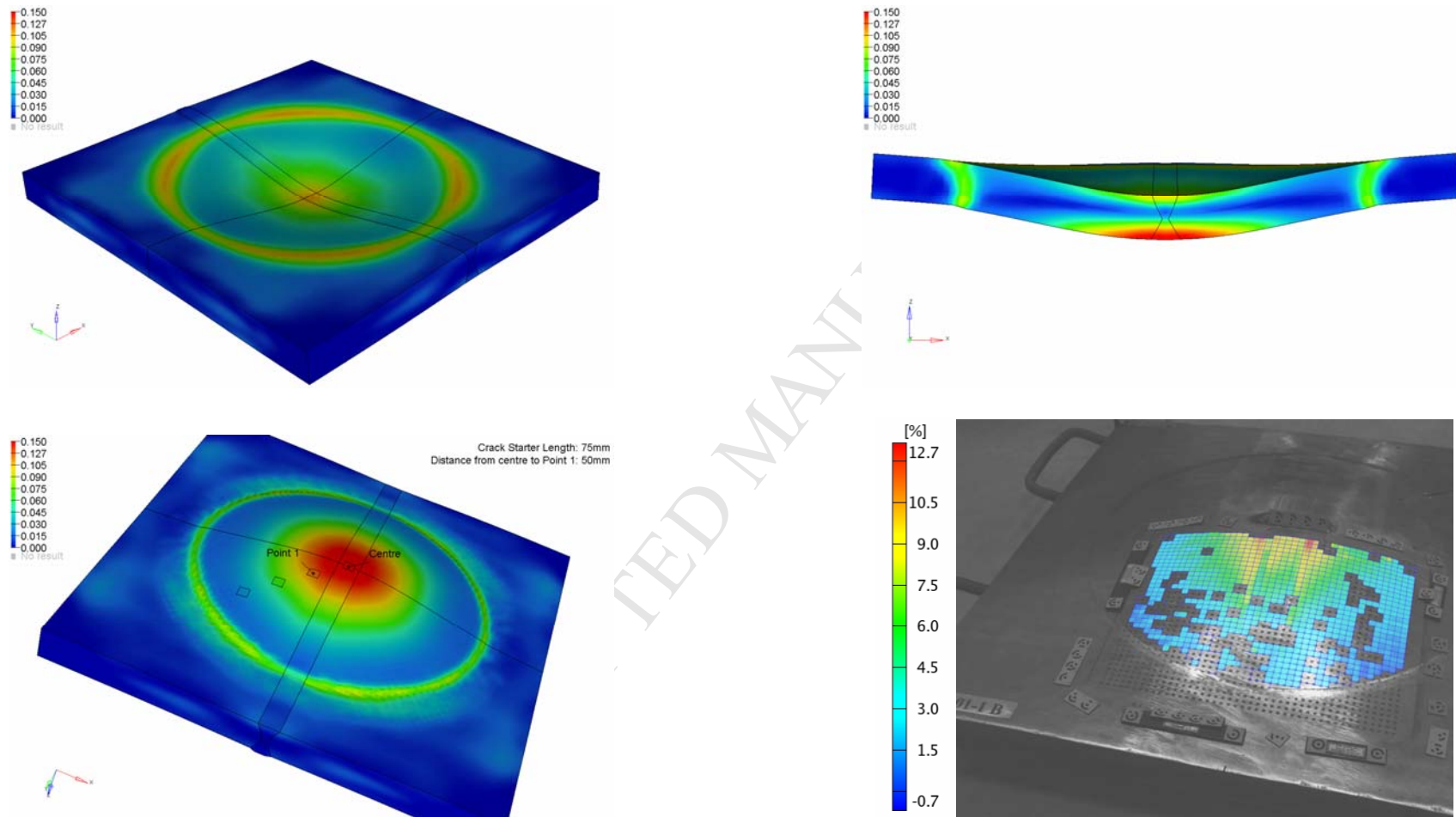
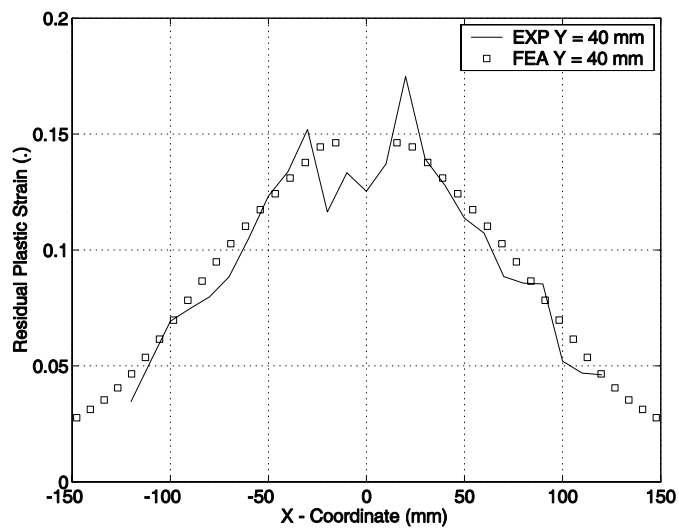
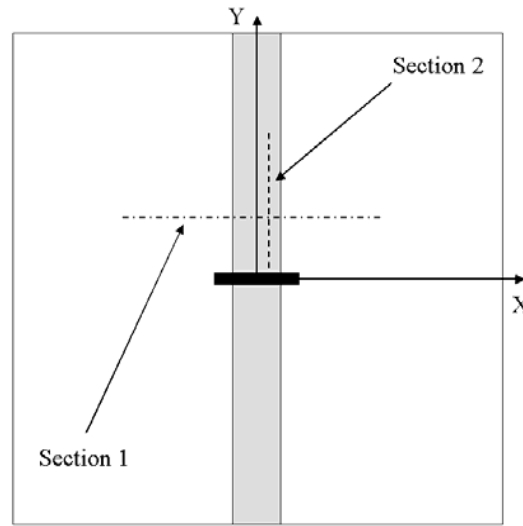


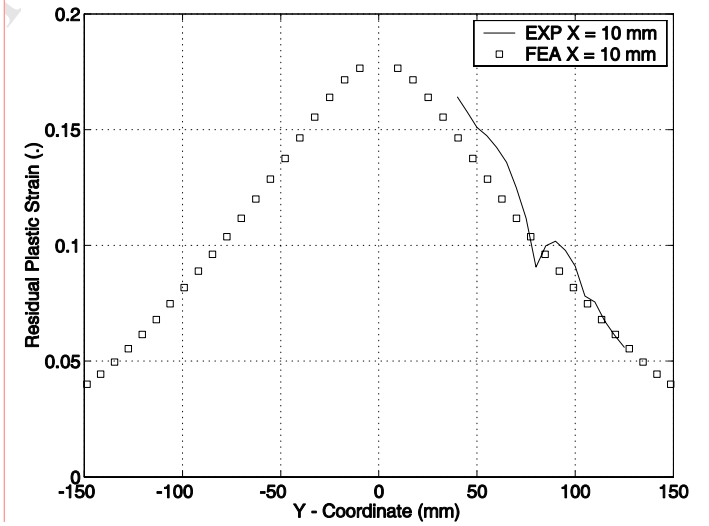
Figure 5. Residual strain distribution after the first explosion (FEA: plastic strain – experiment: major strain).



(a) section 1



section position



(b) section 2

Figure 6. Residual plastic strain comparison (ECST n°1).

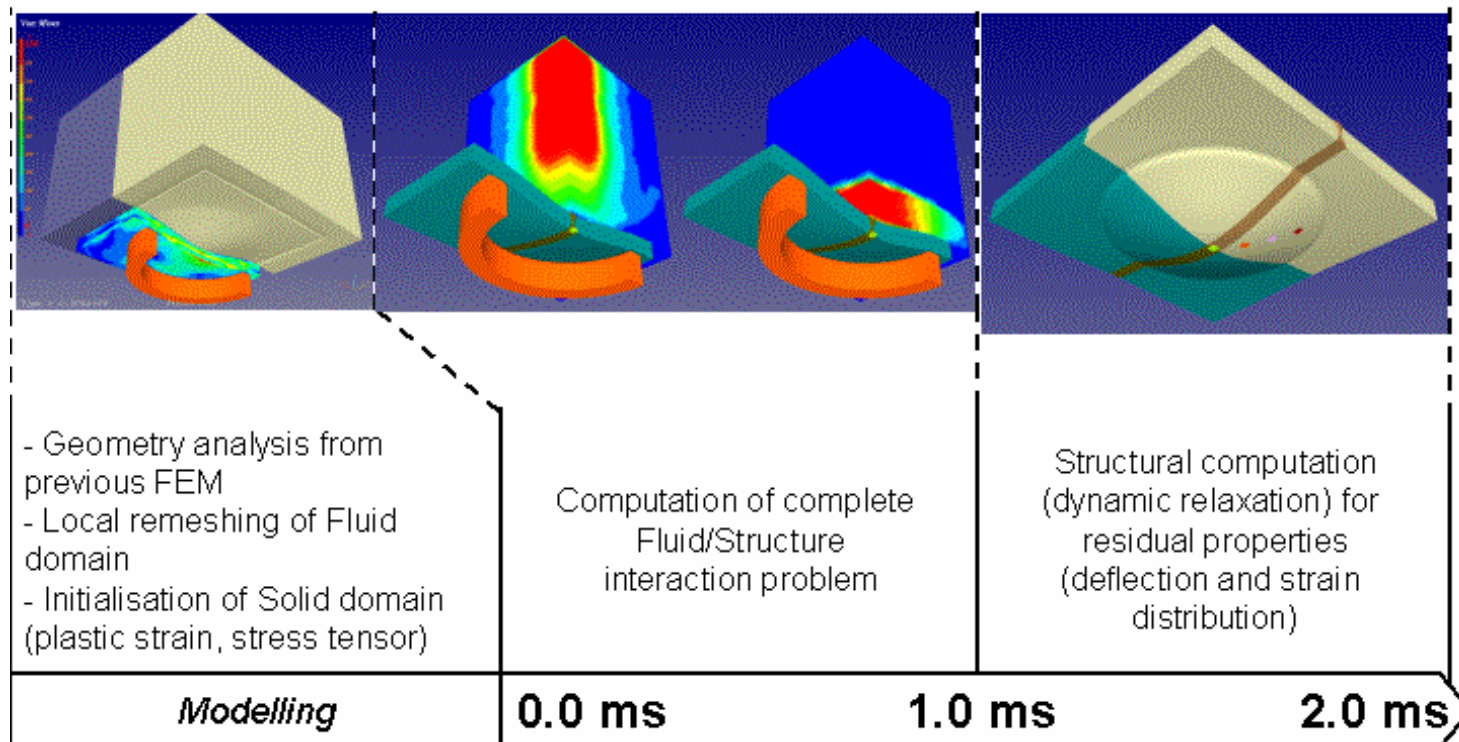


Figure 7. Methodology for second ECST simulation.

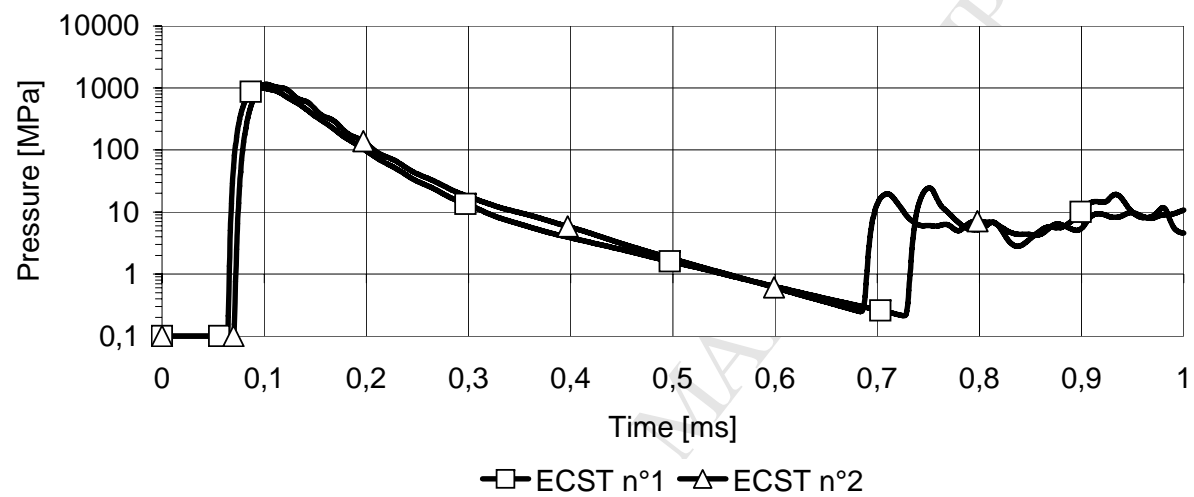


Figure 8. Pressure field measured at the target centre.

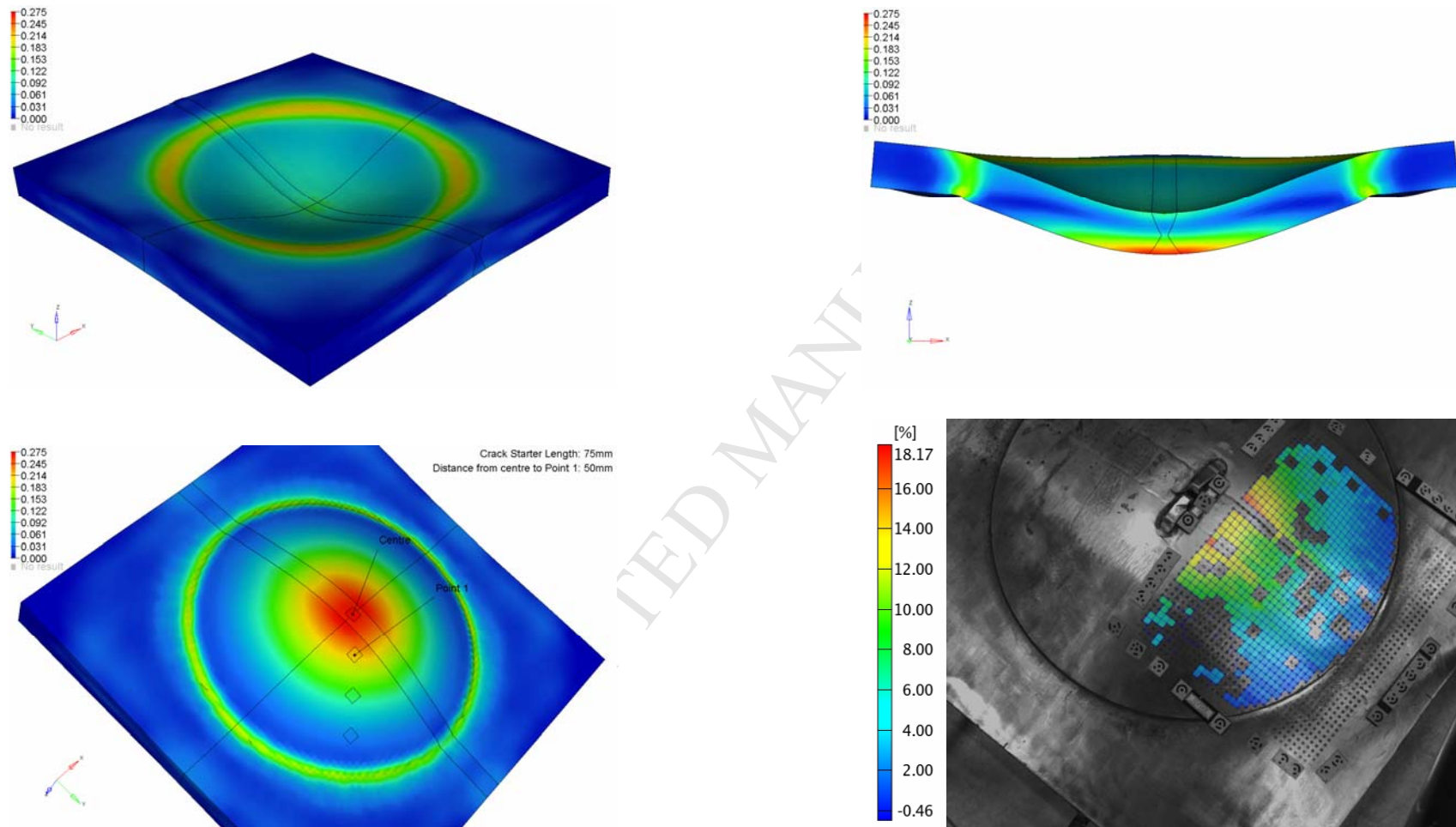


Figure 9. Residual strain distribution after the second explosion (FEA: plastic strain – experiment: major strain).

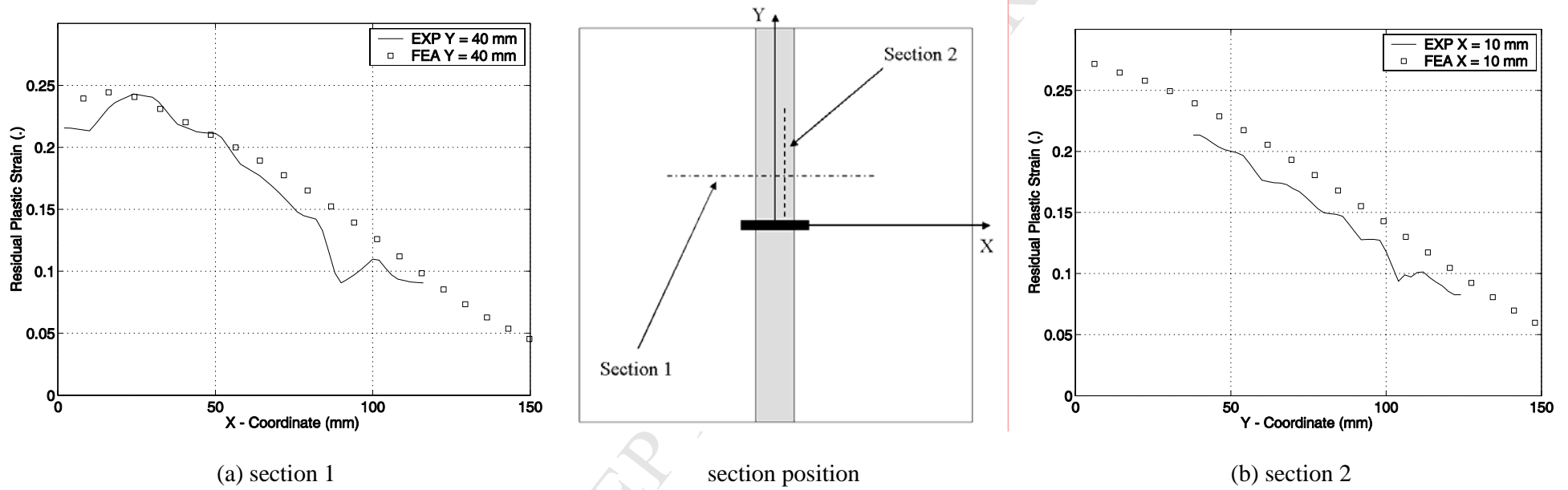


Figure 10. Residual plastic strain comparison (ECST n°2).

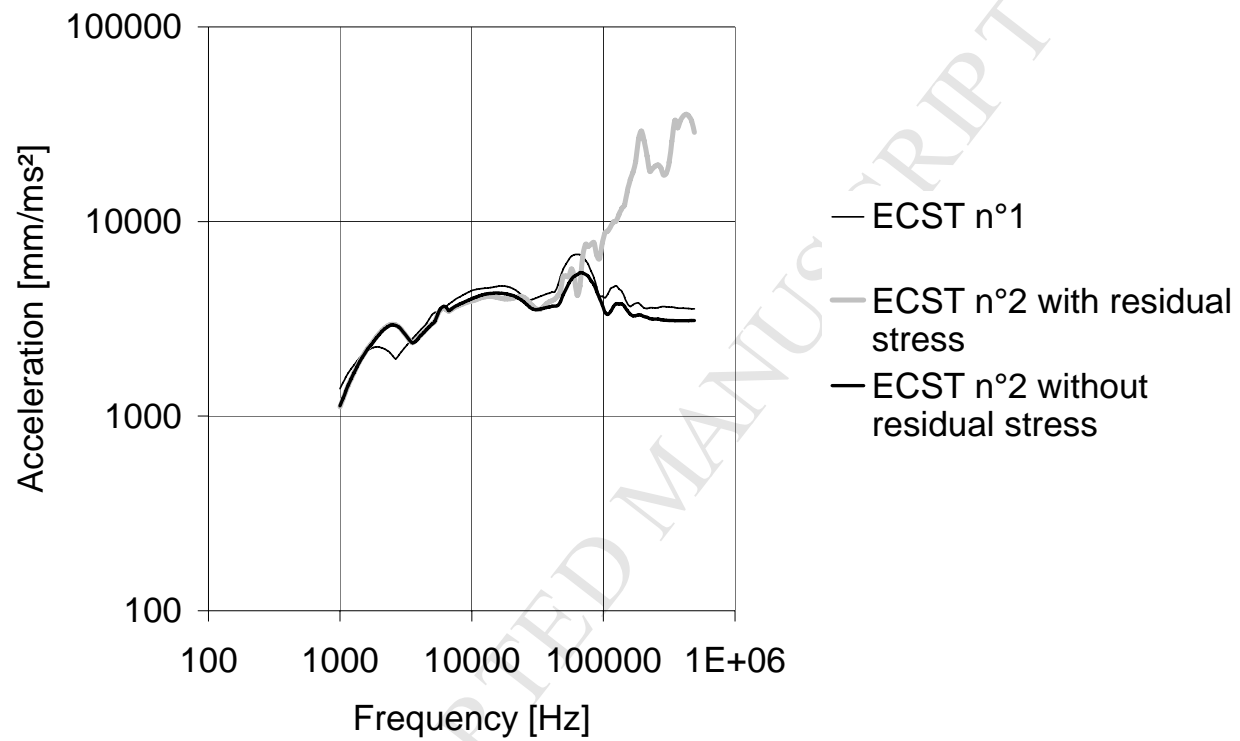


Figure 11. Influence of residual properties on shock spectrum.

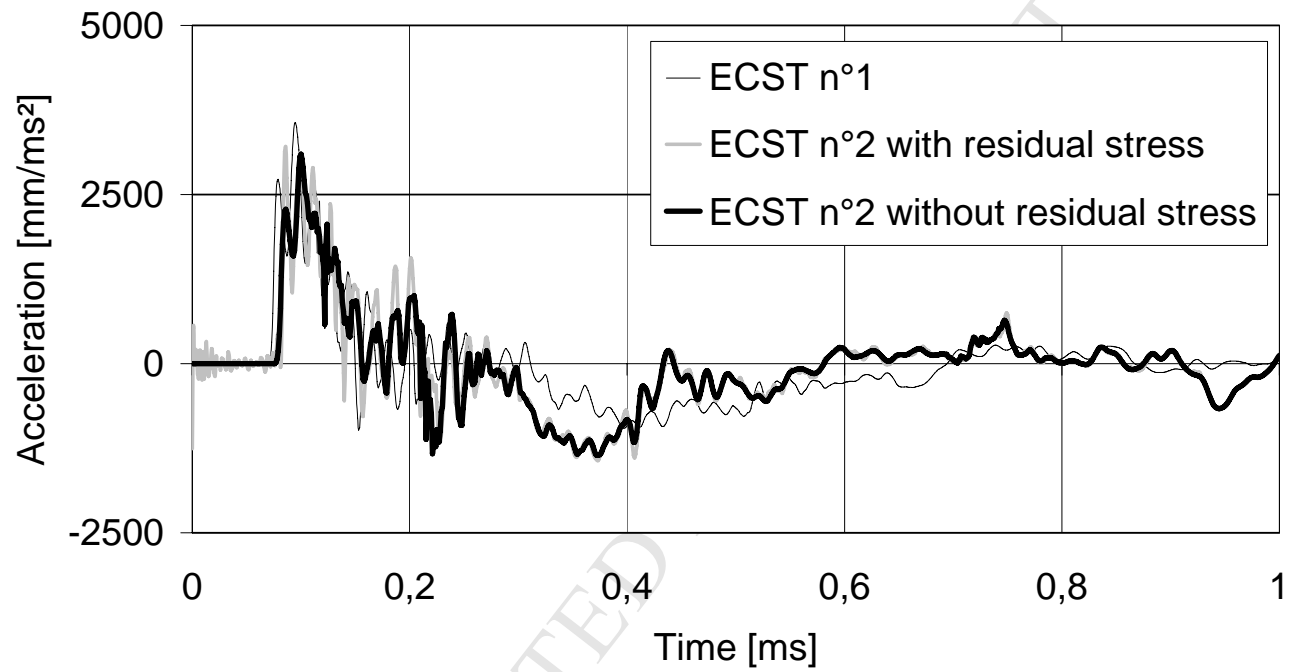


Figure 12. Influence of residual properties on acceleration time history.

List of Tables

Table 1. ECST and BET acceptance criteria [1].

Table 2. Fluid material parameters.

Table 3. Viscoplastic parameters of welded materials.

ACCEPTED MANUSCRIPT

Table 1. ECST and BET acceptance criteria [1].

Explosion tests Acceptance criteria	1 st shot	2 nd shot	Additional shots
Crack starter shall crack	X	N/A	N/A
No piece shall be thrown out of the material being tested	X	X	X
No through thickness cracks shall be present	X	X	N/R
No cracks shall extend into the hold-down area	X	X	X
Percent reduction in thickness	Recorded for information		

Table 2. Parameters of Fluid materials

Explosive (JWL EOS)		Air (Hydrodynamic EOS)
$\rho = 1.5 \text{ g/cm}^3$		$\rho = 1.3 \cdot 10^{-3} \text{ g/cm}^3$
$A = 6.25 \text{ Mbar}$	$B = 0.233 \text{ Mbar}$	$\gamma = 1.4$
$R_1 = 5.25$	$R_2 = 1.6$	$C_0 = C_1 = C_2 = C_3 = 0$
$\omega = 0.25$	$E = 0.0856 \text{ Mbar}$	$C_4 = C_5 = 0.4$
$D_{cj} = 0.745 \text{ cm}/\mu\text{sec}$	$P_{cj} = 0.22 \text{ Mbar}$	$E_0 = 2.5 \cdot 10^{-6} \text{ Mbar}$

Table 3. Viscoplastic parameters of welded materials.

Material					
	(MPa)	(MPa)		(ms ⁻¹)	
Base Material	706	545	0.5	$5 \cdot 10^{-4}$	0.036
Fusion Zone	780	493	0.5	$5 \cdot 10^{-4}$	0.024